

The Benefits and Challenges of Differential Phase Contrast Imaging for Material Science

Iwan JERJEN^{*}, Vincent REVOL^{**}, Christian KOTTLER^{**}, Rolf KAUFMANN^{**},
Claus URBAN^{**}, Thomas LUETHI^{*}, and Urs SENNHAUSER^{*}

^{*}Empa, Swiss Federal Laboratories for Materials Science and Technology,
Ueberlandstrasse 129, CH-8600 Dübendorf, Switzerland

(iwan.jerjen@empa.ch)

^{**}Photonics Division, Centre Suisse d'Electronique et Microtechnique SA,
Technoparkstrasse 1, CH-8005 Zurich, Switzerland

Abstract. X-ray differential phase contrast imaging (DPCI) with a Talbot-Lau interferometer setup allows the simultaneous measurement of the spatial distribution of the real and imaginary part of the refractive index and of the locations of scattering centers of an object. Since the real part of the refractive index of X-rays is several orders of magnitude more important than the imaginary part phase contrast images of weakly absorbing samples show considerably better contrast than conventional attenuation contrast images (ACI). The possibility to obtain better image quality at lower radiation dose raised a lot of interest in the medical and science life communities.

In contrast, the advantages of DPCI for material science are not yet well established. One reason are the difficulties encountered in producing the required phase and absorption grids for high energies (>50 keV). Other reasons are that the well-established ACI already delivers excellent results and that the radiation dose is almost never an issue in material science. Nevertheless, it is expected that DPCI imaging might have some advantages in characterizing light materials, e.g. fibre-reinforced plastics. Remarkably, the sensitivity of dark field imaging to scattering centres smaller than the pixel size allows measuring small cracks and voids invisible to conventional ACI. One application envisaged is the visualization of the transport of fluids in a porous media.

In this paper, a short summary of the theoretical background of ACI and DPCI will be given. The difficulties in developing a DPCI instrument for high energies (> 50 keV) will be outlined. The possible benefits of DPCI for material science will be illustrated with examples. Finally, some sources of artefacts in DPCI will be discussed and compared to artefacts in ACI.

1. Introduction

X-ray computed tomography (CT) is a valuable tool for non-destructive testing (NDT) [1]. X-ray CT is used, for example, in medicine, life science, material science and for failure analysis. The technique is applied at synchrotrons, which produce coherent, highly brilliant X-ray beams, for measuring small samples (~ 1 mm) with spatial resolutions in the order of tens of nanometers. Making use of small X-ray tubes emitting incoherent and broad-band X-ray beams with small focal spot size (~ 1 µm) and a cone beam setup, CT can reach spatial resolution in the order of micrometers. For making X-ray CT measurements of larger and denser samples, X-ray tubes with high energy (~ 450 kV acceleration voltage) or even linear accelerators with energies up to a few MeV are used as X-ray source.



Conventionally, X-ray CT is executed by measuring the attenuation of an incoming X-ray beam. However, X-rays are not only absorbed in a material, but also refracted. It is therefore possible to measure the phase changes which the X-rays experience in the object to be tested. Phase contrast (PC) measurements are standard measurements at synchrotron beam lines [2]-[4]. However, PC CT using conventional X-ray tubes is difficult because the emitted X-rays are incoherent. In 1992, Clauser et al. proposed to use a Talbot-Lau interferometer setup for differential phase contrast (DPC) measurements [5]. A grid placed next to the source has the effect of creating a series of virtual sources which have a sufficient spatial coherence to enable phase measurements. A grid placed behind the sample under test splits the X-ray beam into two out-of-phase beams which interfere with each other to create an interference pattern. The modulation of this interference pattern can be retraced with the help of an absorbing grid which has a corresponding periodicity. At the time, the idea was demonstrated with an optical source. Indeed, it is technologically challenging to produce thick grids with small openings, i.e. with a high aspect ratio. In 2006, Pfeiffer et al. demonstrated that it is possible to record DPC images with low-brilliance X-ray sources, too [6]. Ever since, DPC imaging with a Talbot-Lau interferometer excited the scientific community [7][11].

2. Theoretical Background

The interaction of X-rays with matter can be described with a complex refractive index [12][13]:

$$n = 1 - \delta - i\beta = 1 - \frac{r_0}{2\pi} \lambda^2 \sum_q n_q f_q(0, E), \quad (1)$$

where $1 - \delta$ and β are the real and imaginary part of the complex refractive index n , respectively. r_0 is the classical electron radius, λ is the wavelength, n_q is the number of atoms of type q per unit volume and $f_q(0, E)$ is the complex forward atomic scattering factor for atom q . Both, the real and imaginary part of f_q are a function of the atomic photoabsorption cross section $\mu_a(E)$ and related to each other by a modified Kramers-Kronig relation [12][13].

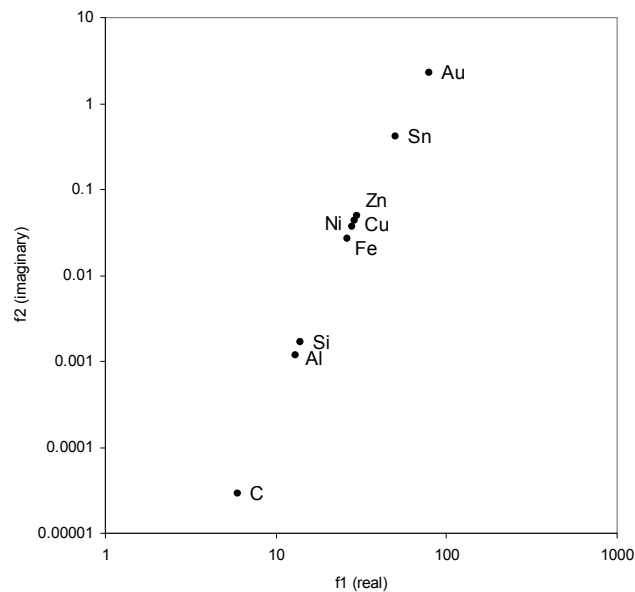


Fig. 1. Real and imaginary parts of the complex forward atomic scattering factors of selected elements for an photon energy of 99.7 keV [12][13].

Fig. 1 shows the real and imaginary parts of the complex forward atomic scattering factors of selected elements. The chosen photon energy of ~ 100 keV corresponds to the mean energy of a typical CT measurement of electronic circuits. As is evident from the huge difference in the imaginary values, the light materials like C, Si and Al will be difficult to detect in the AC image if they are hidden behind dense metals.

With a Talbot-Lau interferometer it is possible to measure the attenuation and the refraction of an X-ray beam passing through an object, simultaneously. Indeed, a phase grid divides the incoming beam into two out-of-phase beams which interfere with each other and create periodic interference patterns at the Talbot distances [3][5][6]. The mean value, phase and amplitude of the interference pattern are measures of the attenuation, the refraction and the coherence loss experienced by an X-ray beam passing through the test object.

The attenuation of the X-ray beam is given by:

$$\ln \frac{I_0(y,z)}{I(y,z)} = \left(\int \mu(l) dl \right)_{(y,z)}, \quad (2)$$

where $I_0(y,z)$ and $I(y,z)$ are the mean values of the interference pattern measured without and with test object. The line integral of the linear attenuation coefficient $\mu(l)$ is taken along the path of the X-ray beam. (y,z) are the pixel coordinates. The refraction angle α is obtained from a modified form of the equation given in [7]:

$$\alpha = \frac{\lambda}{2\pi} \frac{\partial \Phi(y,z)}{\partial y} = \frac{\partial}{\partial y} \left(\int \delta(l) dl \right)_{(y,z)}, \quad (3)$$

where $\Phi(y,z)$ is the phase shift of the X-rays at the plane of the phase grid G_1 . The measured phase shift of the interference pattern φ is related to α by:

$$\varphi = 2\pi \frac{\alpha d}{p_2}, \quad (4)$$

where d is the distance between the phase grid G_1 and the absorption grid G_2 , and p_2 is the spatial period of the absorption grid. The amplitude of the interference pattern, which is a measure of the coherence loss of the X-ray beam and is linked to scattering centres in the object, is governed by a logarithmic law similar to the attenuation [14].

Since the attenuation, the refraction and the coherence loss are given by line integrals, it is possible to reconstruct the three-dimensional distribution of the attenuation coefficient $\mu(x,y,z)$, the decrement of the real part of the refractive index $\delta(x,y,z)$ and the scattering centers $\varepsilon(x,y,z)$ with standard reconstruction algorithms [1],[10],[11],[15]. Yet, one has to bear in mind two things: The integration of the differential phase contrast signal is done in the Fourier space during the filtering operation [7]. And the scattering signal, approximated here by $\varepsilon(x,y,z)$, depends on the orientation of the scattering centres relative to the X-ray beam.

3. Experimental Setup

All measurements presented in this paper were executed with a cone-beam DPC CT setup installed at CSEM. The setup consists of an X-ray tube from COMET (MXR-160HP 20, operated at 40 kV acceleration voltage) with a focal spot size of ~ 1 mm², a flat panel detector from Radicon (Shad-o-Box 2048, Scintillator Min-R 2190) with 2048 x 1024 pixels of 48 x 48 μ m² size, a rotational table from Owis (DMT 65), and a Talbot-Lau interferometer made of three grids which were produced at CSEM in Neuchatel. **Fig. 2** depicts a scheme of the setup:

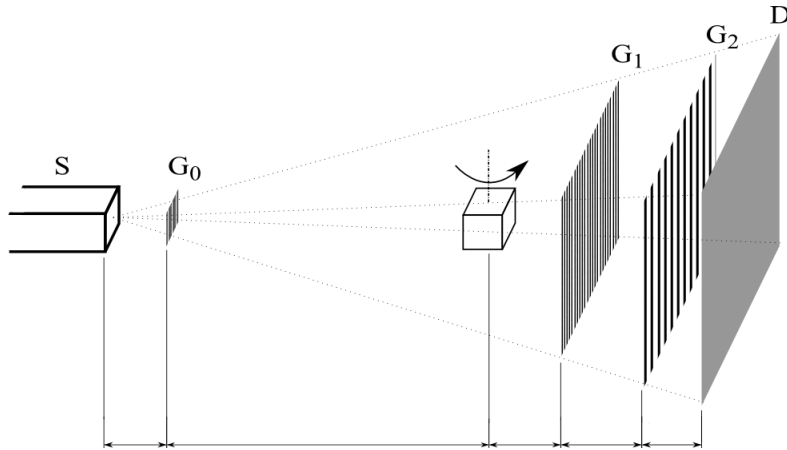


Fig. 2. Scheme of a cone-beam DPC measurement setup: S denotes the X-ray source, D the detector. The source grid G_0 , the phase grid G_1 and the analyzer grid G_2 constitute the Talbot-Lau interferometer. The test sample is placed between the source grid and the phase grid.

The grid G_0 which is placed at the X-ray source alters the incoherent X-ray beam into a series of individual sources which are spatially coherent. The phase grid G_1 splits the X-ray beam into two out-of-phase beams which interfere with each other. The shape of the interference pattern can be sampled by translating the absorber grid G_3 in front of the detector [5]. Table 1 lists the grid parameters.

Table 1. Grid parameters

grid name	material	thickness [μm]	pitch [μm]	duty cycle
G_0	gold	60	57	0.5
G_1	silicium	12.7	2.85	0.5
G_2	gold	30	3	0.3

4. High Energy Differential Phase Contrast Imaging

In material science, the samples under test are often dense and their size can exceed tens of millimeters. For example, the study of materials with structures of different size requires a region of interest which is bigger than several times the maximal structure size. Therefore, CT in material science requires high X-ray energies (~ 100 keV). Thus, the impact of DPCI measurements in material science will be limited unless the energy range where it can be used is extended considerably. This implies the construction of absorber grids of high aspect ratios (>100), i.e. with periods in the order of micrometers and with structure heights in the order of several hundred micrometers. **Fig. 1** shows the spectrum of an X-ray tube which is typical for material science measurements. The transmission curves of three Au layers, 0.03, 0.24 and 0.48 mm thick, are also shown. Only grids with structure heights of >0.5 mm absorb enough to be suitable in a DPCI setup. Yet, to the knowledge of the authors, the maximal structure heights realised so far are in the order of ~ 0.1 mm.

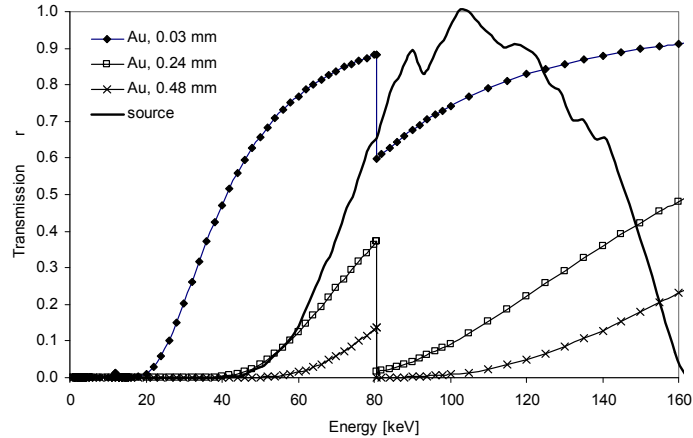


Fig. 3. Transmission of gold layers which are 0.03, 0.24 and 0.48 mm thick as a function of energy. The simulated spectrum of an X-ray tube is also shown (160 kV acceleration voltage, transmission target with 3 μ m W and 2.5 mm Cu filter).

5. X-ray Attenuation and Phase Contrast Imaging

The attenuation and the phase contrast depend on differences in either the density of materials or in their composition (see formula 1)11. The real and imaginary parts of the complex forward atomic scattering factor vary strongly near of absorption edges. Thus, differences in AC and DPC are expected at the corresponding energies. At energies high enough to make the sample under test virtually invisible, the AC signal may be buried in the noise and the DPC will be better. The reason is that even if an X-ray beam is barely attenuated it is still refracted. And interferometers are designed to detect even very small changes of beam directions.

Fig. 4 shows a comparison of AC and DPC CT images of a mouse tissue packed into paraffin and surrounded by oil. Only the DPC allows differentiating between paraffin and oil:

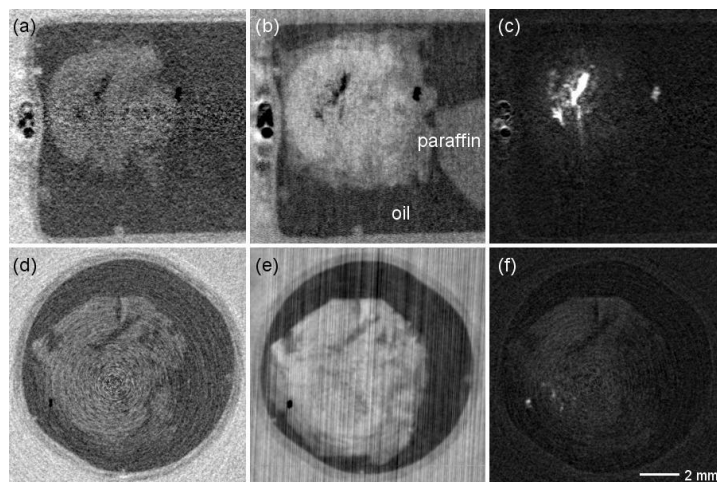


Fig. 4. DPC measurement of mouse tissue [11]. The tissue is packed into paraffin and put into a bin filled with oil. The measurement was executed in a water bath. The top and bottom rows show slices through the reconstructed 3D images orientated perpendicular to each other. (a) and (d) show AC images, (b) and (e) DPC images, and (c) and (f) dark field images. The paraffin and oil can be differentiated in the DPC images, solely.

6. Dark-field Imaging

Local scattering centres which are smaller than the spatial resolution of the DPC CT instrument may scatter the X-rays in arbitrarily directions. Then the local coherence of the beam is destroyed, resulting in a collapse of the interference pattern. Actually, the ratio of the amplitude of the interference pattern to the mean value is a measure of the coherence of the X-ray beam and thus also of the numbers of scattering sites in the sample under test. This so called dark-field imaging is therefore very sensitive to local scattering centres which can be several times smaller than the spatial resolution.

Fig. 5 shows the AC, DPC and dark-field images of bricks which are wet, dry or drying:

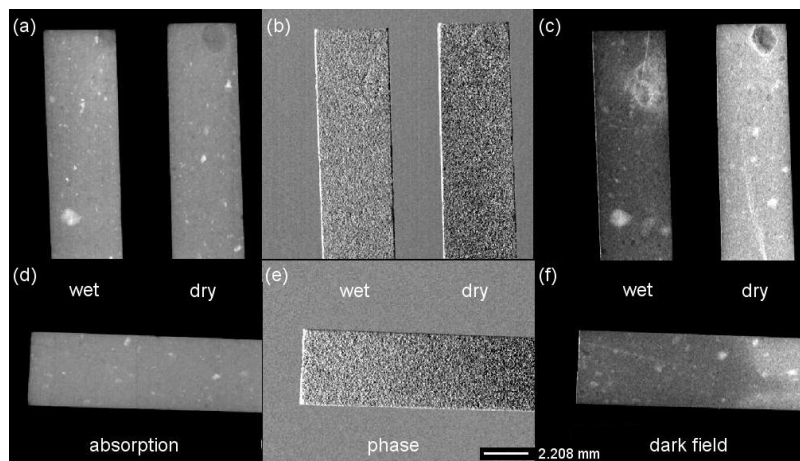


Fig. 5. DPC measurement of water inside bricks: The AC, DPC and dark-field images are shown on the left side (a and d), the centre (b and e) and the right side (c and f), respectively. The top row (a, b, and c) shows the comparison between a wet and a dry brick, the bottom row (d, e, and f) shows the water diffusion inside a single brick [11].

Inclusions of more or less dense materials in the brick can be observed clearly in the AC image. However, it is impossible to locate the water inside the bricks. The DPC images show some difference between wet and dry regions. However, only the dark-field images show the water distribution clearly. This can be explained as follows: The bricks have a lot of voids smaller than the spatial resolution of the measurements. If these voids are filled with air then the X-rays will be scattered strongly at the air-brick interfaces and the dark-field signal is huge. If the voids are filled with water, which has a different refractive index, then the X-rays are refracted much less and the dark-field signal is small.

7. Artefacts in Differential Phase Contrast Imaging

As in conventional AC CT, artefacts may appear in DPC CT images. Since the phase of the interference pattern created by a Talbot-Lau interferometer depends on the energy, a hardening of the X-ray beam in the test object will affect the DPC measurement. The effect is analogous to the well-known beam-hardening artefacts in AC CT and can be corrected for test objects made of a single, homogenous material [16].

In addition, there are DPC CT specific artefacts which origin lies in the nature of phase measurements: The obtained differential phase value may be wrapped, i.e. actual phase values are all mapped into a range between $-\pi$ and $+\pi$. Another source of error is differential phase clipping which occurs whenever the phase changes within one pixel of the recorded DPC image. **Fig. 6** shows a projection of a DPC CT measurement of a piece of

aluminium (**Fig. 6 a**): The DPC signal is wrapped and clipped near of the edges. The erroneous DPC values result in severe artefacts in the reconstructed image (**Fig. 6 b**).

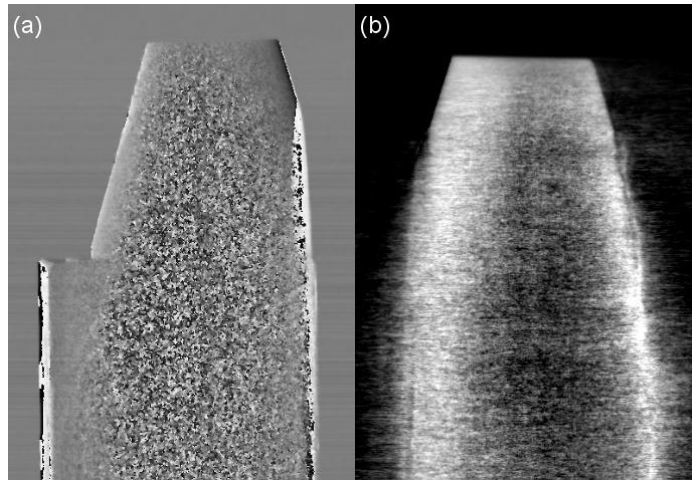


Fig. 6. DPC CT measurement of two pieces of Al welded together: the projection image (a) shows that at the edges of the sample the differential phase values are wrapped and clipped. These errors affect the reconstructed DPC image seriously: The spatial resolution is reduced considerably (b).

8. Conclusions

DPC CT with a Talbot-Lau interferometer is well-suited for analyzing and characterizing materials. This new method shows its advantages in situations where conventional AC CT fails: Light materials which are almost transparent at the energy of the given experiment can be differentiated in the DPC image. And structures below the spatial resolution of the setup are visible in the dark-field image. This allows for example measuring the water transport in bricks which, previously, was solely possible by neutron CT.

However, DPC CT will become an important tool in material science and non-destructive testing only if the energy range is extended. This goal requires the production of high aspect ratio (> 100) grids. In addition, methods have to be developed to correct DPC CT specific artefacts.

If the mentioned difficulties can be overcome then DPC CT will become a valuable imaging tool in non-destructive testing and material science.

References

- [1] A. C. Kak and M. Slaney, *Principles of Computerized Tomography* (IEEE, New York, 1987).
- [2] A. Momose, "Phase-sensitive imaging and phase tomography using X-ray interferometers," *Opt. Express* **11**, 2303-2314 (2003).
- [3] T. Weitkamp, A. Diaz, C. David, "X-ray phase imaging with a grating interferometer," *Opt. Express* **13**, 6296-6304 (2005).
- [4] A. Momose, W. Yashiro, Y. Takeda, Y. Suzuki, T. Hattori, "Phase tomography by X-ray Talbot interferometry for biological imaging," *Jpn. J. Appl. Phys.* **45**, 5254-5262 (2006).
- [5] J. F. Clauser and M. W. Reinsch, "New theoretical and experimental results in Fresnel optics with applications to matter-wave and X-ray interferometry," *Appl. Phys. B* **54**, 380-395 (1992).
- [6] F. Pfeiffer, T. Weitkamp, O. Bunk, and C. David, "Phase retrieval and differential phase-contrast imaging with low-brilliance X-ray sources," *Nature Physics*, vol. **2**, 258-261 (2006).
- [7] F. Pfeiffer, C. Kottler, O. Bunk, C. David, "Hard X-ray phase tomography with low-brilliance sources," *Phys. Rev. Letter* **98**, 108105 (2007).

- [8] C. David, T. Weitkamp, F. Pfeiffer, A. Diaz, J. Bruder, T. Rohbeck, A. Groso, O. Bunk, M. Stampanoni, P. Cloetens, "Hard X-ray phase imaging and tomography using a grating interferometer," *Spectrochimica Acta Part B* **62**, 626-630 (2007).
- [9] F. Pfeiffer, M. Bech, O. Bunk, P. Kraft, E. F. Eikenberry, C. Brönnimann, C. Grünzweig, C. David, "Hard X-ray dark-field imaging using a grating interferometer," *Nature Materials* **7**, 134-137 (2008).
- [10] I. Jerjen, V. Revol, C. Kottler, T. Luethi, U. Sennhauser, R. Kaufmann, C. Urban, "Phase contrast cone beam tomography with an X-ray grating interferometer," *AIP Conf. Proc.* **1236**, 227-231 (2010).
- [11] I. Jerjen, V. Revol, C. Kottler, T. Luethi, U. Sennhauser, R. Kaufmann, C. Urban, "Differentielle Phasenkonstrasttomographie: Eine vielversprechende Methode für die zerstörungsfreie Prüfung," *Conf. Proc. Industrielle Computertomografie*, Wels, Austria (2010).
- [12] B. L. Henke, E. M. Gullikson, and J. C. Davis, "X-ray interactions: photoabsorption, scattering, transmission, and reflection at E=50-30000 eV, Z=1-92," *At. Dat. Nucl. Dat.Tab.*, vol. **54**, 181-342 (1993).
- [13] C. T. Chantler, "Theoretical Form Factor, Attenuation and Scattering Tabulation for Z=1-92 from E=1-10 eV to E=0.4-1.0 MeV," *J. Phys. Chem. Ref. Data*, vol. **24**, 71-643 (1995).
- [14] Z.-T. Wang, K.-J. Kang, Z.-F. Huang, and Z.-Q. Chen, "Quantitative Grating-Based X-Ray Dark-Field Computed Tomography," *Appl. Phys. Letters*, **95**, 094105, (2009).
- [15] L. A. Feldkamp, L. C. Davis, J. W. Kress, "Practical cone-beam algorithm," *J. Op. Soc. Am.* **1**, 612-619 (1984).
- [16] M. Chabior, T. Donath, C. David, O. Bunk, M. Schuster, C. Schroer, F. Pfeiffer, "Beam hardening effects in grating-based x-ray phase-contrast imaging," *Med. Phys.*, **38**, 1189-1195 (2011).